Stress imaging by guided wave tomography based on analytical acoustoelastic model

Abdellahi Abderahmane,[1,a)] Alain Lhémery,[1,b)] and Laurent Daniel[2,c)]

[1]*Université Paris-Saclay, CEA, LIST, Palaiseau, F-91120, France*

[2]*Université Paris-Saclay, CentraleSupélec, CNRS, Group of Electrical Engineering-Paris (GeePs), Gif-sur-Yvette, F-91192 France*

ABSTRACT:

A nondestructive method (M) for stress characterization in plate-like structures is proposed. In this method, the acoustoelastic effects (AEEs) on Lamb and shear horizontal guided waves are used to reconstruct a nonuniform multiaxial stress field. The development of M starts by deriving an analytical acoustoelastic model (An-AEM) to predict AEEs induced by a triaxial stress tensor as a function of the stress components, its orientation, the wave propagation direction, and three acoustoelastic coefficients (AECs). The AECs are independent of stress but specific to each mode. The An-AEM allows one to retrieve the three components of the stress tensor and its orientation from AEEs, assuming the stress to be uniform in the plane of the plate and through its thickness. To deal with stress that is nonuniform in the plane, the An-AEM is combined with time-of-flight straight ray tomography to enable stress field reconstruction. Numerical simulation is used to illustrate how such reconstruction can be performed. It is shown that in some cases, stress components can be reconstructed with arbitrary accuracy, and in other cases, the tensorial nature of stress renders the accuracy of its reconstruction dependent on spatial variations of the stress orientation. © 2022 Acoustical Society of America. https://doi.org/10.1121/10.0010359

I. INTRODUCTION

Mechanical stress is a second-order tensor that describes internal forces in a given material.[1] It may originate from thermal, chemical, and/or mechanical loading. It affects structures in two distinct ways. First, it modifies the mechanical state of the structure. On the one hand, this can be detrimental to the structure and may cause its deformation or premature failure.[2,3] On the other hand, it can be intentionally induced in a structure to prevent the aforementioned effects.[4,5] Second, it modifies the physical properties of the structure. Owing to its tensorial nature, stress can induce anisotropy of physical properties.[6–8] It is of great interest to have methods for stress characterization. Those found in the literature can be classified into two different categories. The methods of the first category exploit effects of stress on the mechanical state. They can be either destructive, semi-destructive (layer removal,[9] sectioning,[10] contour method,[11] hole drilling,[12] deep hole,[13] etc.), or nondestructive (diffraction of x ray[14] or neutrons[15]). The methods of the second category exploit effects of stress on the physical properties (all are nondestructive), such as micromagnetic effects (eddy current[16] and magnetic Barkhausen noise[17]), acoustoelastic effects (AEEs; on bulk[18] or surface waves[19]), and photoelastic[20] effects. The domains of applicability of these methods vary greatly and range from those applicable only to uniform uniaxial stress to those applicable to nonuniform multiaxial stress. A closer look at the nondestructive methods shows that they are often *local* (e.g., diffraction methods) or otherwise assume uniform stress (e.g., acoustoelastic methods assuming stress uniformity along the wave propagation path). These limitations prevent them from treating efficiently complex problems.

One of these problems is discussed in the present paper (denoted p_0 subsequently). It consists of determining a multiaxial nonuniform stress tensor field in metallic plates (but uniform through the thickness). To the best of our knowledge, there is no practical solution in the literature to deal with such a problem (whether it is because the problem is outside the domain of applicability of a method or because the use of a given method would be too costly). Thence, the objective of this work is to propose a new method (denoted M) that overcomes the limitations of those found in the literature. The method M shall be nondestructive, nonlocal, and able to characterize multiaxial stress. A method relying on AEEs as a result of multiaxial stress on Lamb and shear horizontal (SH) guided waves, as described in Ref. 21, can fulfill all of these requirements.

This paper is organized as follows. In Sec. II, the problem p_0 and the method of solution M are defined. In Sec. III, an approximate analytical version of the complete acoustoelastic model (AEM; Ref. 21) is derived. The main goal of this version is to make it easier to solve p_0. In Sec. III A, a numerical simulation is used to identify the domain of applicability of the approximate analytical model. In Sec. III B, a

a)Also at: Université Paris-Saclay, CentraleSupelec, CNRS, Group of Electrical Engineering-Paris (GeePs), Gif-sur-Yvette, F-91192 France.
b)Electronic mail: alain.lhemery@cea.fr
c)Also at: Sorbonne Universite, CNRS, Group of Electrical Engineering-Paris (GeePs), Paris, F-75252, France.

simpler version of p_0 (denoted p_{00}) is solved using this analytical version. It consists of retrieving the three stress components and its orientation from the velocity changes when stress is uniform in the plane and through the thickness of the plate. In Sec. IV, a tomographic imaging technique is presented with which M is rendered *nonlocal*. The problems that may arise when the object to be characterized is a tensor are pointed out. In Sec. V, the problem p_0 is decomposed into five problems of increasing difficulty. Numerical simulations are used to delineate the domain of applicability of M. Throughout the paper, bold notation is used for vectors and tensors.

II. DEFINITIONS OF p_0 AND M

A multiaxial nonuniform stress field $\boldsymbol{\sigma} = \mathrm{diag}(\sigma_1, \sigma_2, \sigma_3)$ is present in a metallic plate and assumed to be uniform through its thickness (see Fig. 1). $R_0(\boldsymbol{e}_1, \boldsymbol{e}_2, \boldsymbol{e}_3)$ is a Cartesian frame of reference, and $\boldsymbol{e}_3$ and $\boldsymbol{\sigma}_3$ are normal to the surface of the plate. The local orientation of the stress tensor is, thus, defined by a single angle, denoted by $\alpha = (\boldsymbol{e}_1, \boldsymbol{\sigma}_1)$. The problem p_0 is defined as characterizing the stress tensor field when all three components $(\sigma_1, \sigma_2, \sigma_3)$ and orientation (α) of the stress tensor are dependent on the position (x_1, x_2). Although no work was found in the literature where p_0 was treated by micromagnetic methods (eddy current and Barkhausen noise), there is *a priori* no reason that prevents them from solving p_0 *in principle*. If such methods existed, they would remain, nonetheless, impractical because they are *local* (i.e., allowing for the information to be retrieved only in a small sensor-sized volume). In addition, they could only be implemented for conductive and/or magnetic materials. The acoustoelastic methods[18,19] are less restrictive (no need for the material to be conductive and/or magnetic). However, those found in Refs. 18, 19, 22, and 23 consider the stress to be uniform along the wave propagation path and its orientation to be uniform and known. These limitations render them impractical for solving p_0. The most complex but still simpler version of p_0 treated in the literature is that considered by Dorfi *et al.*,[22] where the stress tensor field is biaxial

FIG. 1. (Color online) A schematic representation of a multiaxial nonuniform stress $\boldsymbol{\sigma}$ in a plate. The reference frame $R_0(\boldsymbol{e}_1, \boldsymbol{e}_2, \boldsymbol{e}_3)$ is defined with $\boldsymbol{e}_3$ normal to the plate, and the stress orientation in the $(\boldsymbol{e}_1, \boldsymbol{e}_2)$ plane is defined by the angle $\alpha = (\boldsymbol{e}_1, \boldsymbol{\sigma}_1)$. The stress components and orientation are functions of (x_1, x_2) and constant through the thickness.

(σ_1, σ_2) with known and uniform orientation. The authors used a grid of transducers (emitting and receiving bulk waves) at the surface of a plate to determine the stress field. A further investigation into the underlying assumptions of the known residual stress characterization methods found in the literature shows that two methods, neutron-diffraction[24] and synchrotron x-ray diffraction,[25] are able to solve p_0. However, these methods suffer from being *local*, time-consuming (measurements in six independent directions are needed to uniquely determine the local value of the stress tensor), and difficult to implement on the field because of the expensive and somewhat cumbersome equipment involved (neutron source or high energy x-ray source).

Here, a *nonlocal*, fast, nondestructive, and easy-to-implement method (M) is proposed, allowing for stress characterization in large regions far from transducers, based on AEEs on elastic guided waves.[21] The nonlocal and fast features of M are ensured by making use of the time-of-flight (TOF) tomography technique, specifically employing long-distance propagating Lamb and SH guided waves. The configuration of M is shown in Fig. 1, where a set of transducers encircles a region of interest R. For a guided mode M (Lamb or SH) of wave vector $\boldsymbol{k}$, the propagation direction is defined by the angle $\beta = (\boldsymbol{e}_1, \boldsymbol{k})$ and the TOF between two transducers S_i and S_j is denoted by t_{ij}^M. The goal is, therefore, to take advantage of the dispersive and multimodal nature of Lamb and SH guided modes[21] to reconstruct the multivariable and directional object $\boldsymbol{\sigma}$ from the t_{ij}^M measurements.

III. ANALYTICAL ACOUSTOELASTIC MODEL (AN-AEM)

A prerequisite for tomography (the technique necessary to develop M) is a physical law that gives the object to be imaged (in this case, the stress tensor) as a function of the measured quantity (t_{ij}^M). Such laws exist in the literature (Refs. 18, 19, 22, and 23) for bulk and surface waves, theoretically derived from the theory of acoustoelasticity, and given as mathematical expressions. A similar theoretical derivation cannot be carried out in the case of Lamb and SH guided waves. For this reason, the present work is based on what was performed in Ref. 21, where a numerical AEM was derived from the theory of acoustoelasticity applied to Lamb and SH guided waves. The development of the AEM starts by giving the stiffness tensor of an isotropic material subjected to multiaxial stress as

$$c_{ijkl}^{eq} = c_{ijkl}(E_i + E_j + E_k + E_l + 1) + \sum_{q=1}^{3} \delta_{ik} c_{jlqq} E_q$$

$$+ \sum_{m}^{3} c_{ijklmm} E_m. \tag{1}$$

E_* are the principal strains. Their expressions as functions of the principal stresses are cumbersome and can be found in Ref. 21. c_{ijkl} and c_{ijklmn} denote the second- and third-order
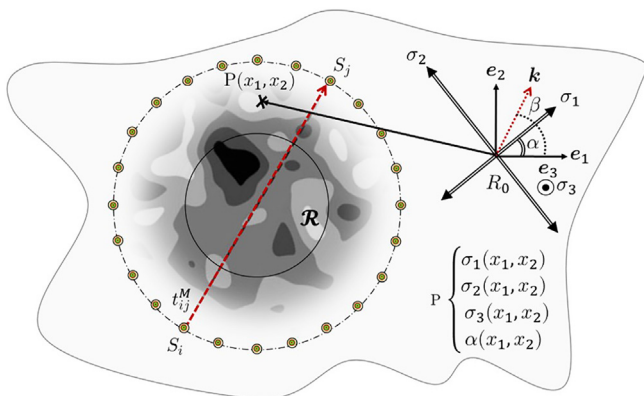
stiffness tensors of the material in its reference state (assumed to be known) and δ_{ik} is the Kronecker function.

This stiffness tensor is then used in a specific development of the semi-analytical finite element method (SAFE; Ref. 26) to predict modal propagation of guided waves in stressed plate. The resulting numerical tool enables one to solve the forward problem consisting of obtaining Lamb and SH wave velocity changes induced by a multiaxial stress tensor. It was shown to accurately predict the experimental results.[21] The AEM has been used to study the forward problem for various loading configurations but cannot be straightforwardly used to solve the inverse problem (i.e., retrieving the stress tensor components and orientation from the induced Lamb and SH velocity changes). This inability stems from two reasons. The first reason is a large number of unknowns in the inverse problem (four), which prevents one from resorting to an inversion using graphs. The second reason is due to the absence of invertible mathematical expressions relating Lamb and SH velocity changes to stress (like those used for bulk waves).

Therefore, the main objective of this section is to obtain such mathematical expressions. For this, the following quantity is defined:

$$\Delta_r v(\boldsymbol{\sigma}) = 100 \times \frac{(v(\boldsymbol{\sigma}) - v_0)}{v_0}, \tag{2}$$

which is the relative velocity change (in percent) of a given mode (Lamb or SH) between two states of the material: a reference state, which is not necessarily stress-free, but where the velocity v_0 is known, and a current state with unknown stress $\boldsymbol{\sigma}$. In what follows, $\Delta_r v(\boldsymbol{\sigma})$ is referred to as the AEE.

The three main findings of Ref. 21 are (1) AEE depends on the mode (Lamb-symmetric, Lamb-antisymmetric, and SH), the velocity considered (group or phase), and the orientation of the stress tensor; (2) AEE is, in general, nonlinearly dependent on the stress components; and (3) AEE induced by a multiaxial stress tensor differs from the sum of AEEs induced by each component considered separately. These results allow one to describe the AEM using the following mathematical expression found by a Taylor series expansion of the multivariable function, $\Delta_r v(\sigma_1, \sigma_2, \sigma_3, \beta - \alpha)$:

$$\Delta_r v_{g/p}^M = \sum_{l=1}^{+\infty} \left(\sum_{i}^{3} A_i^{(l)}(f, \beta - \alpha)\sigma_i^l \right)$$
$$+ \sum_{l,m=1}^{+\infty} \left(\sum_{i,j}^{3} B_{ij}^{(l,m)}(f, \beta - \alpha)\sigma_i^l \sigma_j^m \right)$$
$$+ \sum_{l,m,n=1}^{+\infty} \left(\sum_{i,j,k}^{3} C_{ijk}^{(l,m,n)}(f, \beta - \alpha)\sigma_i^l \sigma_j^m \sigma_k^n \right), \tag{3}$$

where $i, j, k \in \{1, 2, 3\}$ and $i \neq j \neq k$, $\Delta_r v_{g/p}^M$ is the relative group/phase velocity change for a given mode M at a frequency f, and a propagation direction β, which is induced by a multiaxial stress tensor $\boldsymbol{\sigma} = \text{diag}(\sigma_1, \sigma_2, \sigma_3)$ of

orientation α. The Taylor series expansion coefficients $A_i^{(l)}$, $B_{ij}^{(l,m)}$, and $C_{ijk}^{(l,m,n)}$ depend on the mode and nature of the velocity considered (group or phase). This dependency was omitted in their notation for conciseness. This expression is non-invertible (it is impossible to find $\sigma_1, \sigma_2, \sigma_3$, and α when $\Delta_r v_{g/p}^M$ are known for all modes). The AEE is, in general, nonlinearly dependent on stress components. A linear approximation is, however, valid for certain modes in some frequency ranges, as shown in Ref. 21. Such an assumption is henceforward made and its domain of validity will be sought for. As a result, Eq. (3) yields

$$\Delta_r v_{g/p}^M \approx A_{1,g/p}^M(f, \beta - \alpha)\sigma_1 + A_{2,g/p}^M(f, \beta - \alpha)\sigma_2$$
$$+ A_{3,g/p}^M(f, \beta - \alpha)\sigma_3. \tag{4}$$

By virtue of symmetries, one sees that

(a) $A_{3,g/p}^M$ does not depend on $\beta - \alpha$ because σ_3 is normal to the plate;

(b) $\Delta_r v_{g/p}^M(f, \beta - \alpha) = \Delta_r v_{g/p}^M(f, \alpha - \beta)$ because the plane $(\boldsymbol{e}_3, \boldsymbol{\sigma}_1)$ is a plane of symmetry for the loading;

(c) $\Delta_r v_{g/p}^M(f, \beta - \alpha) = \Delta_r v_{g/p}^M(f, \beta - \alpha \pm \pi)$ because both planes $(\boldsymbol{e}_3, \boldsymbol{\sigma}_1)$ and $(\boldsymbol{e}_3, \boldsymbol{\sigma}_2)$ are planes of symmetry for the loading; and

(d) for all β and α, one has $A_{2,g/p}^M(f, \beta - \alpha) = A_{1,g/p}^M(f, \beta - \alpha - \pi/2)$ because for Lamb and SH guided waves, there is no intrinsic difference between σ_1 and σ_2 other than their directions, which are perpendicular.

When $\sigma_1 = \sigma_2$, the elastic properties of the material and, consequently, the AEEs are invariant under rotation of axis $\boldsymbol{e}_3$. Thus, the quantity $A_{1,g/p}^M + A_{2,g/p}^M$ is independent of $\beta - \alpha$. We can, therefore, define the quantities $A_{g/p}^M = (A_{1,g/p}^M + A_{2,g/p}^M)/2$ and $Q_{g/p}^M = (A_{1,g/p}^M - A_{2,g/p}^M)/2$, where $A_{g/p}^M$ depends only on f and $Q_{g/p}^M$ depends on both f and $\beta - \alpha$.

To further simplify the expression of $\Delta_r v_{g/p}^M$, one assumes that $Q_{g/p}^M$ can be rewritten as the product of two terms with separated variables $B_{g/p}^M$ and F as $Q_{g/p}^M(f, \beta - \alpha) = B_{g/p}^M(f)F(\beta - \alpha)$. Finally, Eq. (4) becomes

$$\Delta_r v_{g/p}^M = A_{g/p}^M(f)(\sigma_1 + \sigma_2) + B_{g/p}^M(f)F(\beta - \alpha)(\sigma_1 - \sigma_2)$$
$$+ A_{3,g/p}^M(f)\sigma_3. \tag{5}$$

The coefficients $A_{g/p}^M$, $B_{g/p}^M$, and $A_{3,g/p}^M$ are called the acoustoelastic coefficients (AECs), subsequently. They depend on the frequency, mode, and velocity considered (group/phase).

From (b), (c), (d), F is an even and periodic function of period π that satisfies $F(\beta - \alpha - \pi/2) = -F(\beta - \alpha)$. Since there must exist some frequencies where $\Delta_r v_{g/p}^M$ is finite, the function F must be bounded for all values of $\beta - \alpha$. Without loss of generality, $F(\beta - \alpha)$ can be taken in $[-1, 1]$. On this basis, the choice of $F(\beta - \alpha) = \cos(2(\beta - \alpha))$ is made. Such a choice is motivated by the fact that the trigonometric function *cosine* appears not only in the acoustoelastic laws for bulk waves[23,27] but also for Rayleigh[28] and bulk[29] waves

J. Acoust. Soc. Am. **151** (5), May 2022

Abderahmane *et al.*   2865

in weakly anisotropic elastic media (independently of the origin of anisotropy) and was shown to give an accurate fit for experimental results for Lamb waves.[30]

The final form of $\Delta_r v_{g/p}^M$ becomes

$$
\begin{aligned}
\Delta_r v_{g/p}^M = {} & A_{g/p}^M(f)(\sigma_1 + \sigma_2) \\
& + B_{g/p}^M(f)\cos\left(2(\beta - \alpha)\right)(\sigma_1 - \sigma_2) \\
& + A_{3,g/p}^M(f)\sigma_3.
\end{aligned}
\tag{6}
$$

This expression is referred to as the An-AEM, which gives AEE ($\Delta_r v_{g/p}^M$) explicitly as a function of stress. The An-AEM is the basis on which the solution of p_0 is constructed. To identify its domain of applicability [i.e., for which mode and at which frequency does this formula accurately predict results calculated by the AEM, Eq. (3)], the following error is defined

$$
\begin{aligned}
\epsilon_{g/p}^M = {} & \frac{1}{\max(\tilde{I}, I)} \int |\Delta_r v_{g/p}^M(\text{AEM}) \\
& - \Delta_r v_{g/p}^M(\text{An} - \text{AEM})| dX,
\end{aligned}
\tag{7}
$$

where

$$
\tilde{I} = \int |\Delta_r v_{g/p}^M(\text{AEM})| dX
$$

and

$$
I = \int |\Delta_r v_{g/p}^M(\text{An} - \text{AEM})| dX.
$$

dX is equal to $d\sigma_1 d\sigma_2 d\sigma_3 d\beta$, and ϵ is calculated at each frequency. ϵ (by construction in $[0, 1]$) gives an estimate of the deviation between the full AEM and analytical AEM. Other definitions of error were tested: the root mean square error (RMSE) and normalized RMSE. Both are not suitable: the former measures an absolute difference, which makes it dependent on the value of $\Delta_r v$; the latter measures a relative difference but is unbounded, which makes it inadequate to define fixed thresholds.

A. Domain of applicability of An-AEM

The example taken to identify the domain of applicability of An-AEM is that of a 5-mm-thick plate made of Al 6061-T6 (Ref. 31) of density equal to 2704 kg m^{-3} and the elastic properties (in its reference state) given by Table I.

For the adapted SAFE simulation,[21] the plate thickness is discretized using 32, one-dimensional (1D) three-node isoparametric elements, a number determined by numerical experiments to ensure accuracy.

TABLE I. Al 6061-T6 elastic constants at 25 °C.

Constant	λ	μ	l	m	n
in GPa	56.3	27.5	−281.5	−339	−416

Three numerical parametric studies were performed, in which the three fundamental Lamb (A0 and S0) and shear horizontal (SH0) guided modes were investigated. In the first, the plate is subjected to uniform (in-plane and through-thickness) in-plane uniaxial stress σ_1, ranging from −200 to 200 by 20 MPa step, and the stress orientation (α) is set—for simplicity—to zero while the propagation direction (β) was varied from 0° to 180° with 1.8° step, and the frequency (f) varied from 0 to 500 by 5 kHz step. At each (f, σ_1) step, the two AECs involved, $A_{g/p}^M$ and $B_{g/p}^M$, are fitted on the results of the AEM using the least mean square method. The second study is similar to the first, but the plate is now subjected to uniform uniaxial out-of-plane stress σ_3 and the third AEC $A_{3,g/p}^M$ is obtained. These AECs [denoted for the sake of compactness by A, B, and A_n (for $A_{3,g/p}^M$)] are fitted on these two uniaxial cases and used in a third parametric study to compute the deviation ϵ between AEM and An-AEM [Eq. (6)]. In this third study, the plate is subjected to uniform triaxial stress and all three stress components vary from −200 to 200 MPa.

As the technique to be used for rendering M nonlocal is the TOF tomography, only group velocities are of interest in this work. Nevertheless, similar results can be obtained when using phase velocities if required.

Results are shown in Fig. 2. In the first row, the three AECs (in %/MPa) are plotted as functions of the frequency for the three fundamental modes. AECs fitted on uniaxial cases are presented using solid lines inside shaded areas. These areas represent the possible values of AECs if they were fitted on a triaxial case (i.e., the dependence of AECs on stress). In other words, if the shaded area is large, uniaxial loading cannot be used to determine the AEC. Among the three modes, S0 has the largest shaded area that is at its largest in the frequency range [350,500] kHz where S0 is the most dispersive. The S0 mode happens to be, also, the most sensitive because its AECs are the largest. It is worth noting that mode sensitivity was studied as function of mode dispersion and modal displacement in Ref. 21. No simple relationship between modal displacement/dispersion and mode sensitivity was unveiled. However, for any practical case, the mode sensitivity can be routinely assessed using the AEM. Globally, AECs are dispersive where the corresponding mode is also, and A_n has the highest values. In Fig. 2 (d), the deviations ϵ between AEE calculated by the AEM in the triaxial case and those calculated by the An-AEM with the AECs fitted on uniaxial cases are plotted as functions of frequency. To better understand the meaning of these deviations for the accuracy of the An-AEM, two frequencies were chosen: $f_1 = 200$ kHz and $f_2 = 500$ kHz. At the latter frequency, the error is at its highest (0.193); at the former, the error has an intermediate value (0.017). Since AEEs are functions of four parameters $\sigma_1, \sigma_2, \sigma_3$, and β, a single representation is impossible. We chose to represent the worst-case scenario when the values of σ_1, σ_2, and σ_3 lead to the highest difference between the An-AEM and AEM, namely, when $\sigma_1 = -\sigma_2 = -\sigma_3 = -200$ MPa. The AEEs ($\Delta_r v$) were plotted as functions of the propagation
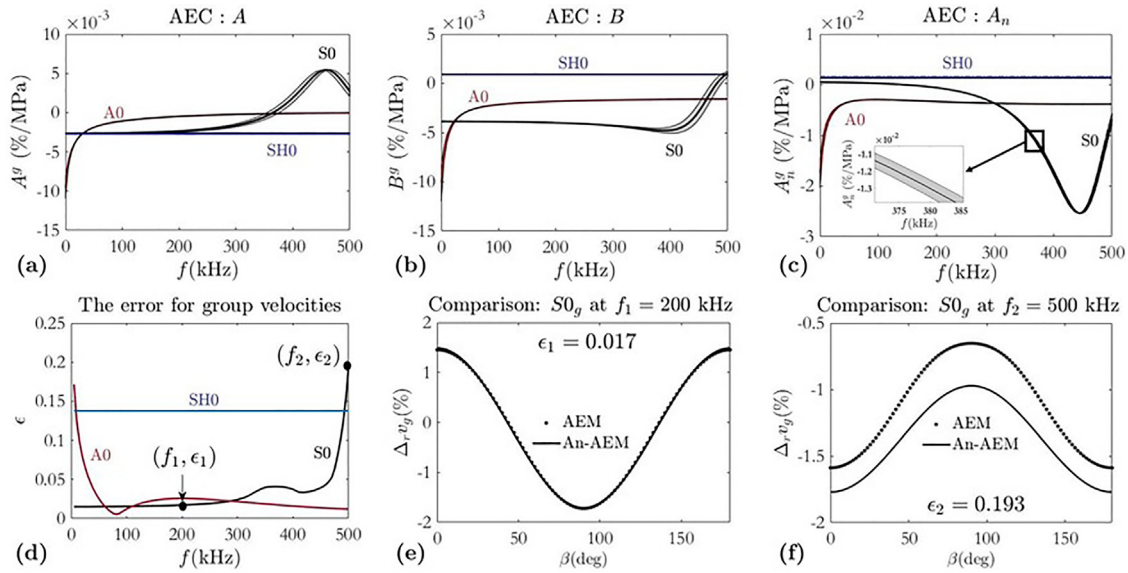
Abderahmane *et al.*

FIG. 2. (Color online) The first row shows the three acoustoelastic coefficients (AECs) for group velocities of the fundamental modes A0, S0, and SH0. The second row shows (d) the deviation between the AEM and An-AEM. (e) and (f) show the relative group velocity change for a loading of $\sigma_1 = -\sigma_2 = -\sigma_3 = -200$ MPa, calculated by the AEM (dotted line) and An-AEM (solid line) at $f_1 = 200$ kHz (e) and $f_2 = 500$ kHz (f).

direction β. Figure 2(e) shows that for the intermediate value of ϵ, the AEM and its analytical version (An-AEM) are indistinguishable. On the other hand, Fig. 2(f) shows that the difference between them can be substantial (same order of magnitude as the AEE) for the highest value of ϵ.

From these results, the domain of applicability of the An-AEM can be defined using the deviation ϵ. For a given mode, the domain is defined as the frequency range(s) in which ϵ is lower than a given threshold ϵ_t. The value given to ϵ_t is not universal and depends on how precise the stress measurement needs to be, which is left to the appreciation of potential end-users. Here, by setting, for example, ϵ_t to 0.15, one gets [0,490] kHz as the domain of applicability for S0, [10,500] kHz for A0, and [0,500] kHz for SH0.

For the sake of generality, no numerical value is given to ϵ_t, and the An-AEM is considered valid at least for S0 and A0 in the frequency range [0,350] kHz (i.e., the range where the AECs of S0 are the least sensitive to stress). In this range, using SH0 is still possible if high precision is not a priority.

A fourth parametric study was conducted—whose results are not given here for conciseness—in which the frequency ranged from 0 to 2 MHz. This study showed that Eq. (6) cannot describe accurately the AEEs for some higher modes at some frequencies. This can be overcome by introducing an extra term [i.e., $C(f)(\cos(4(\beta - \alpha)))$] in the expression of the An-AEM. Increasing the accuracy of the An-AEM comes at the expense of introducing a fourth AEC and a more complicated acoustoelastic law. Simplicity of the An-AEM is important because it is possible *in principle* to obtain these AECs from experiments in the same way as that to obtain them for Rayleigh waves in Ref. 32. Two simple experiments can be conducted to obtain all three AECs. In the first, the plate is subjected to a known uniaxial stress σ_1 (for simplicity, $\alpha = 0°$), and the AEE ($\Delta_r v^M$) for a given mode M at a given

frequency f is measured in two perpendicular directions (e.g., $\beta_\parallel = 0°$ and $\beta_\perp = 90°$). After simple algebra [see Eq. (6)], one obtains

$$A^M(f) = \frac{\Delta_r v^M_\parallel(f) + \Delta_r v^M_\perp(f)}{2\sigma_1}$$

and

$$B^M(f) = \frac{\Delta_r v^M_\parallel(f) - \Delta_r v^M_\perp(f)}{2\sigma_1}. \qquad (8)$$

For A_n, the plate is subjected to uniaxial out-of-plane stress σ_3 and the AEE is measured in any direction,

$$A^M_n(f) = \frac{\Delta_r v^M(f)}{\sigma_3}. \qquad (9)$$

Once the domain of applicability of the An-AEM is determined and the AECs are obtained (numerically or experimentally), solving the problem p_{00} is possible, as presented in Sec. III B.

B. Solving p_{00}

The problem p_{00} (Fig. 3) consists of retrieving the four quantities $\sigma_1, \sigma_2, \sigma_3$, and α from the AEE when stress is uniform in the plane and through the thickness. The An-AEM is used in its domain of applicability. Three transducers S_1, S_2, S_3 form an isosceles right triangle. Since (e_3, σ_1) is a plane of symmetry for the problem, a measurement in a single direction will give *two* possible stress orientations (one being the mirror image of the other). The choice of angles $90°$ and $45°$ gives the solution with the least number of measurements.

To solve p_{00} using this configuration, the transducers are assumed to be able to radiate and detect S0 and A0
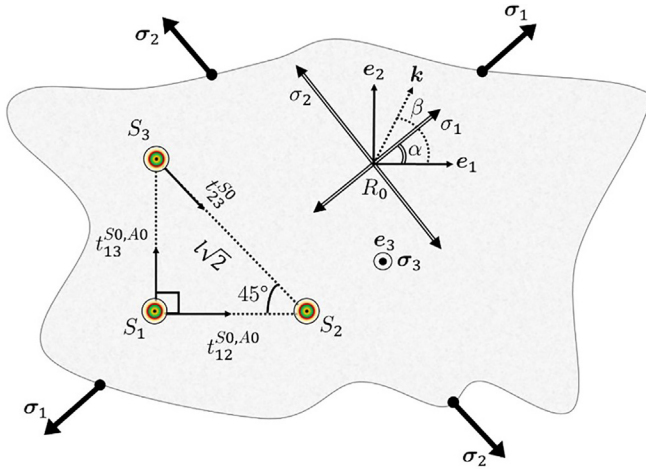
J. Acoust. Soc. Am. **151** (5), May 2022

Abderahmane *et al.*   2867

FIG. 3. (Color online) The measurement configuration of an unknown uniform triaxial stress using three transducers S_1, S_2 and S_3 forming an isosceles right triangle.

modes. A centre frequency f_c is chosen, at which both modes are generated. Two measurements are made.

In the first measurement, S_1 generates both modes, detected by S_2 ($\beta = 0°$) and S_3 ($\beta = 90°$). The different TOFs are denoted by $t_{12}^{S0}, t_{12}^{A0}, t_{13}^{S0}$, and t_{13}^{A0}. By substituting Eq. (2) into Eq. (6), the TOFs are given by

$$
\text{A0}:
\begin{cases}
\dfrac{l}{t_{12}^{A0}} = v_0^{A0} + \dfrac{v_0^{A0}}{100}\Big[A^{A0}(\sigma_1 + \sigma_2) \\
\qquad + B^{A0}\cos(2\alpha)(\sigma_1 - \sigma_2) + A_n^{A0}\sigma_3\Big], \\[2mm]
\dfrac{l}{t_{13}^{A0}} = v_0^{A0} + \dfrac{v_0^{A0}}{100}\Big[A^{A0}(\sigma_1 + \sigma_2) \\
\qquad - B^{A0}\cos(2\alpha)(\sigma_1 - \sigma_2) + A_n^{A0}\sigma_3\Big],
\end{cases}
$$

$$
\text{S0}:
\begin{cases}
\dfrac{l}{t_{12}^{S0}} = v_0^{S0} + \dfrac{v_0^{S0}}{100}\Big[A^{S0}(\sigma_1 + \sigma_2) \\
\qquad + B^{S0}\cos(2\alpha)(\sigma_1 - \sigma_2) + A_n^{S0}\sigma_3\Big], \\[2mm]
\dfrac{l}{t_{13}^{A0}} = v_0^{S0} + \dfrac{v_0^{S0}}{100}\Big[A^{S0}(\sigma_1 + \sigma_2) \\
\qquad - B^{S0}\cos(2\alpha)(\sigma_1 - \sigma_2) + A_n^{S0}\sigma_3\Big],
\end{cases}
\tag{10}
$$

where $v_0^{S0,A0}$ are the velocities known in the reference state. The AECs ($A^{S0,A0}, B^{S0,A0}$, and $A_n^{S0,A0}$) and velocities ($v_0^{S0,A0}$) are taken at f_c. After some algebra, Eq. (10) becomes

$$
\begin{cases}
\sigma_3 = 50\dfrac{A^{S0}\Big[\Big(\dfrac{l}{t_{12}^{A0}}+\dfrac{l}{t_{13}^{A0}}-2v_0^{A0}\Big)\Big]-A^{A0}\Big[\Big(\dfrac{l}{t_{12}^{S0}}+\dfrac{l}{t_{13}^{S0}}-2v_0^{S0}\Big)\Big]}{\big(v_0^{A0}A^{S0}A_n^{A0}-v_0^{S0}A^{A0}A_n^{S0}\big)}, \\[4mm]
\sigma_1 + \sigma_2 = \dfrac{\Big(\dfrac{50}{v_0^{S0}}\Big(\dfrac{l}{t_{12}^{S0}}+\dfrac{l}{t_{13}^{S0}}-2v_0^{S0}\Big)-A_n^{S0}\sigma_3\Big)}{A^{S0}}, \\[4mm]
\cos(2\alpha)(\sigma_1-\sigma_2) = \dfrac{\dfrac{50}{v_0^{S0}}\Big(\dfrac{l}{t_{12}^{S0}}-\dfrac{l}{t_{13}^{S0}}\Big)}{B^{S0}}.
\end{cases}
\tag{11}
$$

In the second measurement, S_3 generates $S0$ detected by S_2 ($\beta = 135°$). One has

$$
\frac{l\sqrt{2}}{t_{32}^{S0}} = v_0^{S0} + \frac{v_0^{S0}}{100}\Big[A^{S0}(\sigma_1 + \sigma_2) \\
- B^{S0}\sin(2\alpha)(\sigma_1 - \sigma_2) + A_n^{S0}\sigma_3\Big].
\tag{12}
$$

Using Eqs. (11) and (12) and recalling that $\alpha \in [0°, 180°]$, the *unique* solution is

$$
\begin{cases}
\alpha = \dfrac{1}{2}\text{atan}\left(\dfrac{\Big(\dfrac{l}{t_{12}^{S0}}-\dfrac{l\sqrt{2}}{t_{32}^{S0}}\Big)+\Big(\dfrac{l}{t_{13}^{S0}}-\dfrac{l\sqrt{2}}{t_{32}^{S0}}\Big)}{\dfrac{l}{t_{12}^{S0}}-\dfrac{l}{t_{13}^{S0}}}\right), \\[4mm]
\sigma_1 = \dfrac{S+D}{2}, \quad \sigma_2 = \dfrac{S-D}{2}, \\[3mm]
S = \dfrac{\Big(\dfrac{50}{v_0^{S0}}\Big(\dfrac{l}{t_{12}^{S0}}+\dfrac{l}{t_{13}^{S0}}-2v_0^{S0}\Big)-A_n^{S0}\sigma_3\Big)}{A^{S0}}, \\[4mm]
D = \dfrac{\dfrac{50}{v_0^{S0}}\Big(\dfrac{l}{t_{12}^{S0}}-\dfrac{l}{t_{13}^{S0}}\Big)}{B^{S0}\cos(2\alpha)}.
\end{cases}
\tag{13}
$$

The AECs appear in the denominators of the expressions of σ_3 [Eq. (11)], S, and D [Eq. (13)]. Care must be taken when choosing the centre frequency to avoid null or small-valued denominators.

It is also possible to solve p_{00} using a single mode (instead of two) generated at two different centre frequencies. Solving p_{00} is a first part of the method M. A second part consists in solving p_0, in which the stress is nonuniform in the plane (but uniform through the thickness).

IV. TOMOGRAPHY FOR STRESS IMAGING

This section focuses on the technique rendering stress characterization *nonlocal*. Let l_0 be the shortest length over which the stress is assumed to be uniform. p_0 could be solved in a similar way to p_{00}, which is by scanning the plate surface with a cluster of three transducers forming an isosceles right triangle whose hypotenuse is shorter than l_0. Such a solution is *local* and can be time-consuming if l_0 is small relative to the size of the region to image. To overcome this, the technique of tomography is used. A set of transducers (emitters and receivers) encircles the region of interest R (Fig. 1). Depending on the ratio of the wavelength λ and characteristic length of the object l_0, two types of tomography are usually defined. For a ratio $\lambda/l_0 \geq 1$, one speaks of diffraction tomography (DT), where the incident wave (from an emitter) is scattered in all directions and detected by the rest of the sensors. DT cannot, *in principle*, solve p_0 because the notions of wave path and propagation direction are lost as the incident wave is scattered in all directions. This prevents it from characterizing tensorial objects, which are defined *uniquely*, only with respect to some direction (in

our case, that of the wave propagation). In contrast, ray tomography (RT) is defined when $\lambda/l_0 \ll 1$. Under this condition, diffraction is negligible, and the wave propagation obeys the Snell-Descartes refraction laws (see Ref. 33). When the propagation takes place in a homogeneous medium, the wave trajectory (called "ray") is straight, and one speaks of straight ray tomography (SRT).[33] Otherwise, the rays are curved, and the technique is referred to as curved ray tomography (CRT).[33] RT is based on ray theory (see Ref. 33), where, in addition to the condition $\lambda/l_0 \ll 1$, l_0 must be smaller than the width of the first Fresnel zone. For isotropic homogeneous media, this width is equal to $\sqrt{\lambda L}$, where L is the distance between the emitter and receiver (the ray length).

Inversion based on RT relies on two fundamental equations:[33] one describes the wave amplitude (transport) and the other describes its velocity (eikonal). Only the latter is used here in the development of M as it defines the TOF $t_{E \to R}$ between the emitter (E) and receiver (R). Its integral form (see Ref. 33 for details) is given by

$$t_{E \to R} = \int_E^R \frac{ds}{v(s)}, \qquad (14)$$

where ds denotes the length element along the ray ($E \to R$) and v is the group velocity. When the contrast between the index of refraction of the object to image and that of the background medium is less than 5%, the ray curvature can be neglected so that SRT applies.[34,35] Here, the object to be imaged is the stress and its refraction index is given by the AEE ($\Delta_r v$), which is smaller than 5%, in general, as shown in Figs. 2(e) and 2(f). Therefore, the TOF SRT is used hereafter to develop M.

To reconstruct an object, SRT can use two algorithms: the filtered back projection (FBP)[35] or the algebraic reconstruction technique (ART).[35] The former is based on the Radon transform[36] and Fourier slice theorem.[35] The FBP has been shown to be more accurate and faster than the ART[35] and is used in M for these reasons. The two main configurations to run this algorithm are the *parallel-beam* and *fan-beam*, which are shown in Fig. 4. Given that M uses RT, its resolution is determined by
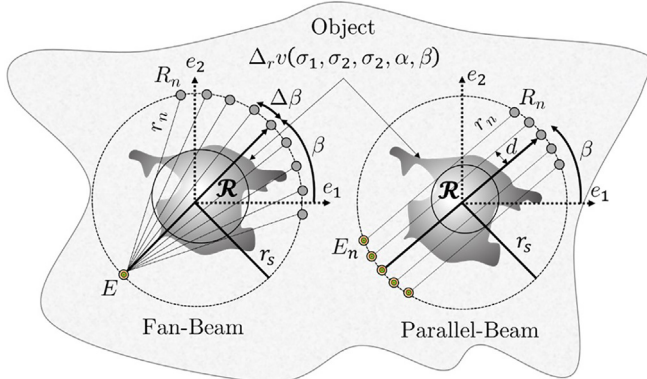

FIG. 4. (Color online) The two FBP configurations used in M (*fan-beam* and *parallel-beam*).

that of RT, which is equal to the width of the first Fresnel zone ($\sqrt{\lambda L}$). Therefore, the shortest distance between two adjacent rays (equal to d for the *parallel-beam* and $r_n \Delta\beta$ for the *fan-beam*) is taken to be less than $\sqrt{\lambda L}$. The region of interest R is defined by the area where the density of ray-intersections is high enough for accurate reconstruction. For the *parallel-beam* (respectively, the *fan-beam*), this region is a circle with a diameter $(n-1)d$ [respectively, $2r_s \sin((n-1)\Delta\beta/2)$], where n is the number of sensors.

In *fan-beam*, there is only one emitter (E) and n receivers (R). The straight line linking E to R_i (receiver number i) is the wave trajectory (ray r_i). The middle ray (thick arrow) makes an angle β with e_1. Other rays are distributed on both sides of the middle ray with an angular step of $\Delta\beta$. One projection corresponds to a single value of β, where the wave(s) radiated by the emitter is(are) received by all of the receivers. In the *fan-beam* version, β varies in the range $[0°, 360°]$. In *parallel-beam*, there are n emitters and n receivers. The rays are parallel and distributed on both sides of the middle ray (thick arrow) with a step d. The middle ray makes an angle β with e_1. One projection corresponds to a single value of $\beta \in [0°, 180°]$, where the wave(s) radiated by E_i is(are) received by R_i for all $i \in \{1, n\}$.

Tomography has been used in the literature with different types of waves to reconstruct various objects. For example, acoustic[34] and elastic bulk[37] waves are used to reconstruct the density, guided waves are used to reconstruct the thickness of plates,[38] and electromagnetic[39] waves (x ray) are used to reconstruct the attenuation/density. In these applications, the physical law relating the measured quantity (TOF, wave amplitude, and intensity) to the object contains a single *scalar* unknown (e.g., thickness or attenuation/density), which is isotropic (i.e., independent of the direction of wave propagation) and, more importantly, *invertible* on a single ray. These characteristics allow tomographic algorithms (FBP or ART) to reconstruct—*in principle*—the object with arbitrary precision. The only errors in the reconstruction stem from ambient noise, temperature fluctuation, uncertainties in the measurement equipment, or in the values of the physical properties of the medium. Such sources of error are not discussed in the present work.

Our main goal is to study how tomography can be used to reconstruct the stress—a tensor—field, based on a law [i.e., the An-AEM, Eq. (6)] that contains four unknowns (σ_1, σ_2, σ_3, and α), is anisotropic (dependent on the propagation direction β) and, more importantly, is *non-invertible* on a single ray. The last characteristic [due to the presence of the *cosine* function in Eq. (6)] arises from the fact that the plane (e_3, σ_1) is a plane of symmetry for the problem. This led to the necessity of using two different propagation directions to have a unique solution for p_{00} (Sec. III B). One can find works in the literature that deal with similar problems. In seismology, a law similar to the An-AEM gives bulk[40] or Rayleigh[41] waves as functions of the earth's elastic anisotropy. Photoelastic tomography[42] was used to assess the residual stress in glass. In Refs. 40 and 41, the problem has more unknowns than equations; as a result, it is treated as an

J. Acoust. Soc. Am. **151** (5), May 2022

Abderahmane *et al.*   2869

optimisation problem. In Ref. 42, the problem is formulated so that only a scalar quantity is measured, assuming the stress orientation to be known and uniform, and then reorienting the specimen such that only a single component of stress is imaged. Here, M takes advantage of the dispersive and multimodal nature of guided waves to formulate a system of equations leading to a unique solution to the problem, as demonstrated in what follows.

V. PROBLEM p_0

The problem p_0, for which M is developed, is treated in five cases of stress distribution of increasing difficulty: uniaxial out-of-plane stress $\boldsymbol{\sigma} = \mathrm{diag}(0, 0, \sigma_3)$, uniaxial in-plane stress $\boldsymbol{\sigma} = \mathrm{diag}(\sigma_1, 0, 0)$, biaxial in- and out-of-plane stress $\boldsymbol{\sigma} = \mathrm{diag}(\sigma_1, 0, \sigma_3)$, biaxial in-plane stress $\boldsymbol{\sigma} = \mathrm{diag}(\sigma_1, \sigma_2, 0)$ and triaxial stress $\boldsymbol{\sigma} = \mathrm{diag}(\sigma_1, \sigma_2, \sigma_3)$, the last two being treated simultaneously.

A. Uniaxial out-of-plane stress

The plate contains a uniaxial out-of-plane stress field. The physical meaning of such stress configuration is questionable due to the free boundary conditions on both sides of the plate. However, the case is formally interesting as the solution is similar to that for thickness or density variations. Indeed, the acoustoelastic law $\Delta_r v_{g/p}^M = A_{n,g/p}^M(f)\sigma_3$ deduced from Eq. (6) by setting $\sigma_1 = \sigma_2 = 0$ contains a single *scalar* unknown (σ_3, the direction being known), is isotropic (independent of β), and invertible on a single ray ($\sigma_3 = \Delta_r v_{g/p}^M / A_{n,g/p}^M$). To reconstruct the map of σ_3, a single mode generated at a single centre frequency suffices. Substituting Eq. (2) into Eq. (6) and the result into Eq. (14), the TOF of that mode (for example, A0) for a given ray r_i is written as

$$t_{r_i}^{A0} = \int_{r_i} \frac{100ds}{100v_0^{A0} + v_0^{A0}A_n^{A0}\sigma_3(s)}. \tag{15}$$

In tomographic inversion, the quantity to be imaged (here, σ_3) is considered constant on a given ray, which yields

$$\sigma_3 = \frac{100}{A_n^{A0}}\left(\frac{r_i}{v_0^{A0}t_{r_i}^{A0}} - 1\right). \tag{16}$$

This formula can be used to reconstruct the stress field from the TOF (t^{A0}). A_n^{A0} being nonzero for all frequencies in $]0, 500]$ kHz (see Fig. 2), the previous expression is always defined, although the centre frequency is better chosen where ϵ is small. To avoid redundancy, the numerical results for this case are not given, since conclusions that can be drawn from them are presented in the next case, which encompasses it.

B. Uniaxial in-plane stress

For this case, the acoustoelastic law is deduced from Eq. (6) by setting $\sigma_2 = \sigma_3 = 0$. One obtains

$$\Delta_r v_{g/p}^M = A_{g/p}^M(f)\sigma_1 + B_{g/p}^M(f)\cos\left(2(\beta - \alpha)\right)\sigma_1. \tag{17}$$

The classical tomographic approach cannot be used anymore because Eq. (17) contains two unknowns (σ_1 and α) and is anisotropic (dependency on β). Furthermore, the law is non-invertible on a single ray: for each position (x_1, x_2) on a given ray r_i, the stress direction can be clockwise or anticlockwise with respect to that of r_i and, in both cases, the TOFs are identical. This last point is one of the shortcomings of M. To reconstruct σ_1 and, if possible, α, one needs to form a system of two equations on each ray. Such a system can be formed using two modes (A0 and S0) generated at a single centre frequency or one single mode generated at two centre frequencies. The former choice is made here leading to the TOF given by

$$\begin{cases} t_i^{A0} = \int_{r_i} \dfrac{100ds}{100v_0^{A0} + v_0^{A0}\left[A^{A0} + B^{A0}\cos\left(2(\beta - \alpha(s))\right)\right]\sigma_1(s)}, \\[4mm] t_i^{S0} = \int_{r_i} \dfrac{100ds}{100v_0^{S0} + v_0^{S0}\left[A^{S0} + B^{S0}\cos\left(2(\beta - \alpha(s))\right)\right]\sigma_1(s)}. \end{cases} \tag{18}$$

The quantities σ_1 and α are considered constant on r_i, which yields

$$\begin{cases} \sigma_1 = 100\dfrac{\left(\left(\dfrac{r_iB^{S0}}{v_0^{A0}t_i^{A0}} - \dfrac{r_iB^{A0}}{v_0^{S0}t_i^{S0}}\right) - (B^{S0} - B^{A0})\right)}{(B^{S0}A^{A0} - B^{A0}A^{S0})}, \\[6mm] \alpha = \begin{cases} \beta + \dfrac{1}{2}\mathrm{acos}\left(\dfrac{100}{v_0^{A0}B^{A0}\sigma_1^*}\left(\dfrac{r_i}{t_i^{A0}} - v_0^{A0}\right) - \dfrac{A^{A0}}{B^{A0}}\right), \\[4mm] \beta - \dfrac{1}{2}\mathrm{acos}\left(\dfrac{100}{v_0^{A0}B^{A0}\sigma_1^*}\left(\dfrac{r_i}{t_i^{A0}} - v_0^{A0}\right) - \dfrac{A^{A0}}{B^{A0}}\right), \end{cases} \end{cases} \tag{19}$$

where σ_1^* is the integral of σ_1 along a given ray r_i divided by its length (r_i). The expression of σ_1 is independent of α. If the centre frequency is chosen such that the denominator is not small/null, then σ_1 can be reconstructed, *in principle*, with arbitrary precision.

On the other hand, the reconstruction of stress orientation α suffers from three problems. First, it depends on σ_1 so that any error in the reconstruction of σ_1 will affect that of α. Second, while the centre frequency can be chosen so that B^{A0} is not small/null, the presence of σ_1^* in the denominator is problematic. This is because if along a given ray, σ_1 is not largely positive (tension) or largely negative (compression), σ_1^* can be small or even null, leading to indefinite expression. When it is the case, such a ray cannot be used in the reconstruction, which leads to loss of information. Third, the major issue with stress orientation is that for each ray, two values are possible, giving the same TOF. Without *a priori* information, there is no reason to favour one over the other.

To better understand these remarks, a numerical study was conducted. Two random distributions (of σ_1 and α)

were generated using a random generator function, applied on two-dimensional (2D) Gaussian functions. Equation (19) can be used in *fan-beam* and *parallel-beam* configurations. The results shown in Fig. 5 were found using the latter. In the first row of Fig. 5, Fig. 5(a) contains the original (object) distribution of $\sigma_1 \in [-100, 100]$ MPa, Fig. 5(b) contains its reconstruction using 33 rays and 18 projections, and Fig. 5(c) contains the error (the difference between the two). Figure 5(d) compares them along a single ray [the black line in Fig. 5(a) and red line in Fig. 5(b)]. In Fig. 5(c), the error is practically null within R but is maximum out of R. Indeed, out of R and close to the transducers, there are not enough ray-intersections to get sufficient information. The comparison on a single ray [Fig. 5(d)] shows that the object and its reconstruction superimpose (with a small deviation outside R). These results confirm that the amplitude σ_1 can be reconstructed, *in principle*, with arbitrary precision as for the uniaxial out-of-plane case treated in Sec. V A but not shown. The second row shows the original distribution of the stress orientation $\alpha \in [30°, 170°]$ [Fig. 5(e)], its reconstruction [Fig. 5(f)], the error [Fig. 5(g)], and the comparison along a single ray [Fig. 5(h)]. Figures 5(g) and 5(h) show that although the distribution is not well reconstructed, it still contains useful information: the overall spatial distribution of the stress orientation is reconstructed but not in detail. In Fig. 5(i), a second simulation was conducted for the same spatial distribution of α in Fig. 5(h), but a smaller range of variation (i.e., $[70°, 120°]$ instead of $[30°, 170°]$)

was assumed. Moreover, the amplitude σ_1 was chosen such that σ_1^* is not null for most rays. From this simulation, only the comparison along one ray is given [Fig. 5(i)], which shows drastic improvement in the reconstruction of the stress orientation.

C. Biaxial in- and out-of-plane stress

This case combines the two previous cases. Here, the acoustoelastic law to be inverted on a given ray is deduced from Eq. (6) by setting $\sigma_2 = 0$. One has

$$\Delta_r v_{g/p}^M = A_{g/p}^M(f)\sigma_1 + B_{g/p}^M(f)\cos(2(\beta - \alpha))\sigma_1(x, y) + A_{n,g/p}^M(f)\sigma_3. \quad (20)$$

It is anisotropic and non-invertible on a single ray and contains three unknowns (σ_1, σ_3, and α). As for the first case, the physical meaning of the present case is also questionable because of the free boundary conditions on both sides of the plate. Nonetheless, the case offers a theoretical framework in which the consequence of a relatively large error ϵ on the reconstruction can be studied. To obtain σ_1, σ_3, and α, a system of three equations is formed. One can use (a) one dispersive mode generated at three different centre frequencies; (b) two modes, where one mode is generated at two different centre frequencies; and (c) three modes generated at a single frequency. The latter choice is made, and all three fundamental modes are used. The TOF expressions become
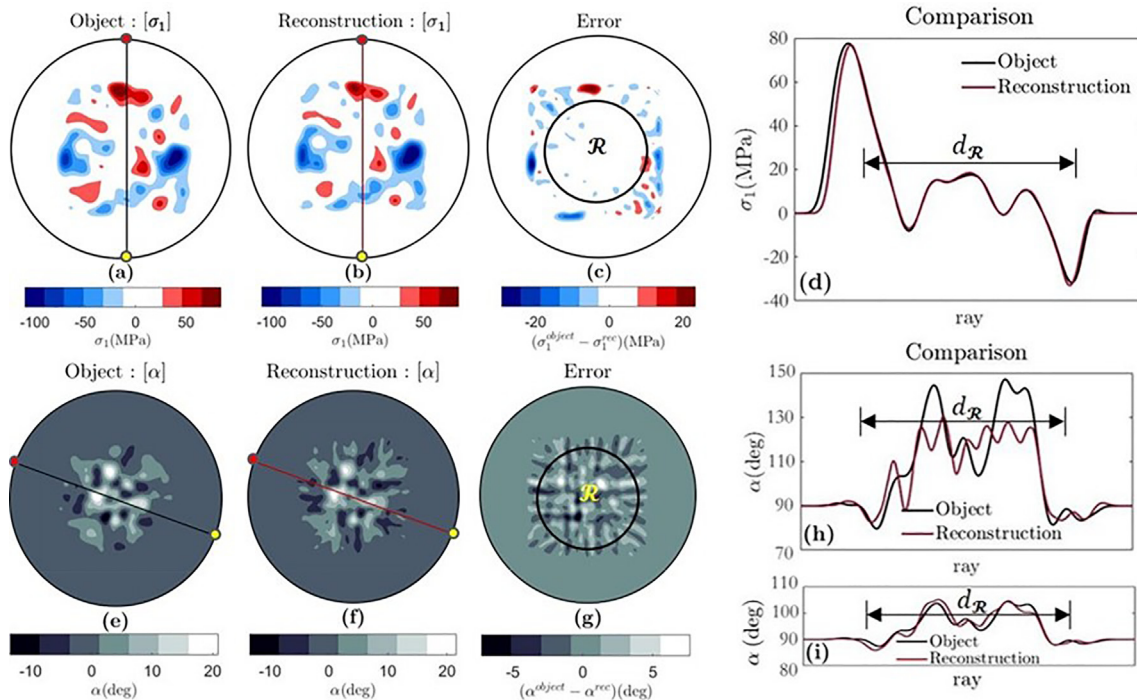

FIG. 5. (Color online) The first row shows (a) the original σ_1 distribution, (b) its reconstruction using 33 rays (emitter-receiver) and 18 projections, (c) the difference between (a) and (b), and (d) the comparison along a single direction [black line in (a) and red line in (b)]. Second row: (e)–(h) same as (a)–(d) but for the distribution of stress orientation α with $\alpha \in [30°, 170°]$, (i) is the same as (h) but for a different simulation assuming a reduced range $\alpha \in [70°, 120°]$. d_R is the diameter of the region of interest R.

J. Acoust. Soc. Am. **151** (5), May 2022

Abderahmane *et al.* 2871

$$
\begin{cases}
t_i^{A0} = \displaystyle\int_{r_i} \frac{100\,ds}{v_0^{A0}\left(\left[A^{A0} + B^{A0}\cos\left(2(\beta - \alpha(s))\right)\right]\sigma_1(s) + A_n^{A0}\sigma_3(s)\right) + 100 v_0^{A0}}, \\[2ex]
t_i^{S0} = \displaystyle\int_{r_i} \frac{100\,ds}{v_0^{S0}\left(\left[A^{S0} + B^{S0}\cos\left(2(\beta - \alpha(s))\right)\right]\sigma_1(s) + A_n^{S0}\sigma_3(s)\right) + 100 v_0^{S0}}, \\[2ex]
t_i^{SH0} = \displaystyle\int_{r_i} \frac{100\,ds}{v_0^{SH0}\left(\left[A^{SH0} + B^{SH0}\cos\left(2(\beta - \alpha(s))\right)\right]\sigma_1(s) + A_n^{SH0}\sigma_3(s)\right) + 100 v_0^{SH0}}.
\end{cases}
\tag{21}
$$

Again, the quantities σ_1, σ_3, and α are considered constant on r_i and an invertible system of two equations, whose unknowns are σ_1 and σ_3, is deduced from Eq. (21). Once this system is solved, the stress orientation is obtained from σ_1. After some algebra, one obtains

$$
\begin{cases}
\sigma_1 = \dfrac{Q(\mathrm{SH0}, A0)\left(B^{S0}f_{A0} - B^{A0}f_{S0}\right) - Q(S0, A0)\left(B^{\mathrm{SH0}}f_{A0} - B^{A0}f_{\mathrm{SH0}}\right)}{Q(\mathrm{SH0}, A0)P(S0, A0) - Q(S0, A0)P(\mathrm{SH0}, A0)}, \\[3ex]
\sigma_3 = \dfrac{P(\mathrm{SH0}, A0)\left(B^{S0}f_{A0} - B^{A0}f_{S0}\right) - P(S0, A0)\left(B^{\mathrm{SH0}}f_{A0} - B^{A0}f_{\mathrm{SH0}}\right)}{Q(S0, A0)P(\mathrm{SH0}, A0) - Q(\mathrm{SH0}, A0)P(S0, A0)}, \\[3ex]
Q(a, b) = B^a A_n^b - B^b A_n^a, \quad P(a, b) = B^a A^b - B^b A^a, \quad f_a = \dfrac{100}{v_0^a}\left(\dfrac{r_i}{t_i^a} - v_0^a\right), \\[3ex]
\alpha = \begin{cases}
\beta + \dfrac{1}{2}\mathrm{acos}\left(\dfrac{A_n^{S0}f_{A0} - A_n^{A0}f_{S0} - \left(A_n^{S0}A^{A0} - A_n^{A0}A^{S0}\right)\sigma_1^*}{\left(A_n^{S0}B^{A0} - A_n^{A0}B^{S0}\right)\sigma_1^*}\right), \\[3ex]
\beta - \dfrac{1}{2}\mathrm{acos}\left(\dfrac{A_n^{S0}f_{A0} - A_n^{A0}f_{S0} - \left(A_n^{S0}A^{A0} - A_n^{A0}A^{S0}\right)\sigma_1^*}{\left(A_n^{S0}B^{A0} - A_n^{A0}B^{S0}\right)\sigma_1^*}\right).
\end{cases}
\end{cases}
\tag{22}
$$

The expression of α shows that its reconstruction still suffers from the same three problems that were mentioned for the previous case. σ_1 and σ_3 are independent of each other and of α and could be reconstructed with arbitrary precision as in the previous cases.

However, it appeared in Fig. 2(d) that the deviation ϵ for SH0 is larger than those for A0 and S0. As a consequence, using SH0 can introduce a small error on the TOF t^{SH0}. To study the effect of using SH0, the maximum deviation between the AEM and An-AEM for SH0 was estimated at 10%. Random errors of this magnitude were added to t^{SH0} for each ray in every projection. A numerical simulation was conducted. To avoid redundancy and focus on the error introduced by the use of SH0, only results for σ_1 are given.

The conclusions drawn from them readily apply to the results for σ_3. The conclusions drawn for α are identical to those of the previous case. Equation (22) is valid for the *fan-beam* and *parallel-beam*. The results appearing in Fig. 6 are obtained using the *fan-beam* with 36 projections and 45 rays in each projection.

Figure 6(c) shows a small error in R but not as small as that in the case appearing in Fig. 5(c). The error in the reconstruction (in R) is around 10%, which is similar to that intentionally added to t^{SH0}. This is not a coincidence and can be easily proven (using Taylor series expansion) from the expression of σ_1 in Eq. (21). The reconstruction of σ_1, as shown in Figs. 6(c) and 6(d), is affected by the choice of SH0. Similar results for σ_3 are obtained but not shown.
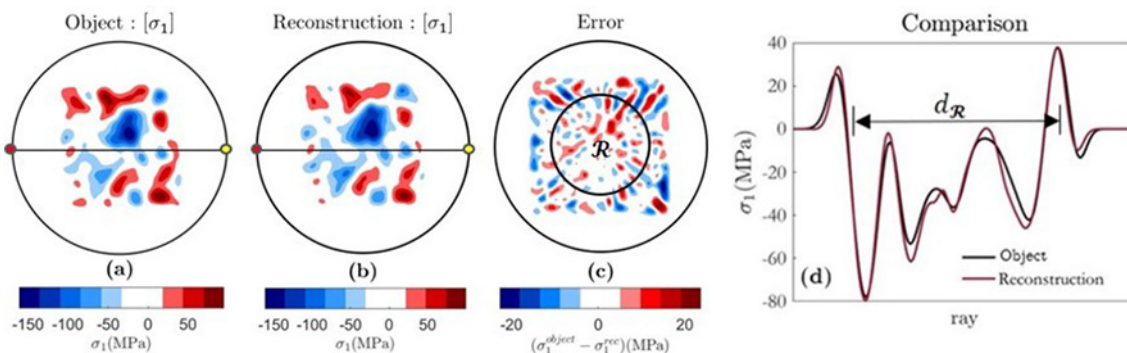

FIG. 6. (Color online) (a) The original σ_1 distribution, (b) its reconstruction using the *fan-beam* (36 projections, 45 rays), (c) the difference between the two, and (d) the comparison along a single ray [black line in (a) and (b)].

2872   J. Acoust. Soc. Am. **151** (5), May 2022

Abderahmane *et al.*

To overcome this, it is possible to use A0 and S0, where the latter is generated at two centre frequencies. In this case, σ_1 and σ_3 can, *in principle*, be reconstructed with arbitrary precision.

D. Biaxial in-plane and triaxial cases

The acoustoelastic law to be inverted on a given ray for the in-plane biaxial case is deduced from Eq. (6) by setting $\sigma_3 = 0$. It is written as

$$\Delta_r v_{g/p}^M = A_{g/p}^M(f)(\sigma_1 + \sigma_2) + B_{g/p}^M(f)\cos(2(\beta - \alpha))(\sigma_1 - \sigma_2). \quad (23)$$

Equation (23) contains three unknowns; it is anisotropic and non-invertible on a single ray. However, contrary to the previous case, which allows an *invertible* system of two equations of unknowns σ_1 and σ_3 on each ray to be formed, here, such a system of unknowns σ_1 and σ_2 cannot be formed anymore. Indeed, both components are affected by the same two coefficients A and $B\cos(2(\beta - \alpha))$. It is, therefore, impossible to obtain σ_1 and σ_2 using only the information from a single ray, independent of the number of modes used on that ray. Only the quantity $S = \sigma_1 + \sigma_2$ can be reconstructed with arbitrary precision using the single ray-approach used so far.

Suppose the two modes A0 and S0 generated at a single centre frequency are used. One can write [after some algebra on Eq. (23)]

$$S = \sigma_1 + \sigma_2$$
$$= 100\frac{\left(\left(\dfrac{r_i B^{S0}}{v_0^{A0} t_i^{A0}} - \dfrac{r_i B^{A0}}{v_0^{S0} t_i^{S0}}\right) - (B^{S0} - B^{A0})\right)}{(B^{S0} A^{A0} - B^{A0} A^{S0})}. \quad (24)$$

This formula is similar to the formula for σ_1 in Eq. (19) and can be used by either *fan-beam* or *parallel-beam*. To obtain σ_1, σ_2, and α, the information must be retrieved from a *collection* of rays that share a common property. In what follows, two cases are treated: (1) when the stress orientation is uniform and (2) when it is not. Only the treatment of the first case is detailed, as the second case is a variant of the first.

1. Uniform stress orientation

Here, the stress orientation α is independent of the position and denoted by α_0. The case is treated in two steps. In the *first* step, the quantity D_β is defined from Eq. (23),

$$D_\beta \equiv \Delta_r v_{g/p}^M - A_{g/p}^M(f)(\sigma_1 + \sigma_2)$$
$$= B_{g/p}^M(f)\cos(2(\beta - \alpha_0))(\sigma_1 - \sigma_2). \quad (25)$$

For a given mode M, D_β is known because $S = \sigma_1 + \sigma_2$ can be reconstructed with arbitrary precision, and $\Delta_r v_{g/p}^M$ is the measured AEE (deduced from the TOF).

D_β has the property of being *null* for particular values of β that are independent of the mode, the frequency but,

more importantly, the ray. These values are $\beta_k = \alpha_0 + (2k + 1)\pi/4, k \in \mathbf{Z}$. As α_0 and β can be taken in $[0°, 180°[$, two possible values of β are in that interval and are perpendicular to each other. Without loss of generality, one can choose $\beta_{0,-1} = \alpha_0 \pm \pi/4$. The *second* step is to identify $\beta_{0,-1}$. To this end, the *parallel-beam* version is the most adequate: for a given projection (β constant), all rays are parallel. Therefore, it is easy to identify the values of β for which D_β is null. Once $\beta_{0,-1}$ have been obtained, α_0 can be deduced, and $\sigma_1 - \sigma_2$ is further given by

$$\sigma_1 - \sigma_2 = \frac{D_\beta}{B^{A0}\cos(2(\beta - \alpha_0))}, \quad (26)$$

where the mode A0 was chosen as an example. With the use of Eq. (24), this yields

$$\begin{cases} \sigma_1 = \dfrac{1}{2}\left(S + \dfrac{D_\beta}{B^{A0}\cos(2(\beta - \alpha_0))}\right), \\ \sigma_2 = \dfrac{1}{2}\left(S - \dfrac{D_\beta}{B^{A0}\cos(2(\beta - \alpha_0))}\right). \end{cases} \quad (27)$$

To retrieve α_0, we define D_β^m as

$$D_\beta^m \equiv \frac{\displaystyle\sum_{r=1}^{n_{\text{rays}}}|D_\beta|}{\displaystyle\max_{p \in \{1, n_{\text{proj}}\}}\left(\sum_{r=1}^{n_{\text{rays}}}|D_\beta|\right)}, \quad (28)$$

which is the sum of the absolute value of D_β (for all rays in a given projection), divided by the largest sum among all projections. By definition, $D_\beta^m \in [0, 1]$ and has the property of D_β of being *null* for particular values of β. The black square markers (D_β^m as function of β) in Fig. 7 show the results for a case where σ_1 and σ_2 vary with position while α_0 was held constant ($\alpha_0 = 55°$). In this example, 18 projections were used (the angular step equals $10°$). For this particular value of α_0, both $\beta_{0,-1}$ are among the set of projection angles,
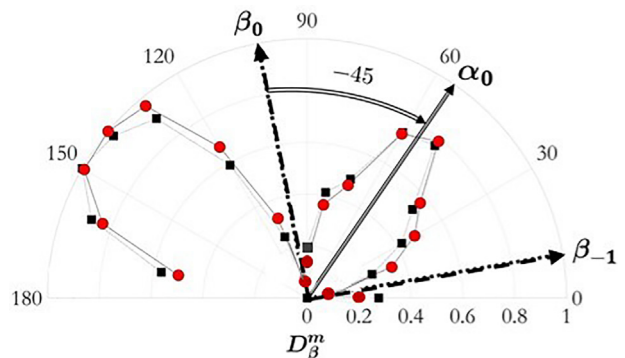

FIG. 7. (Color online) D_β^m as a function of β for uniform stress orientation. Black square markers correspond to the case when the projection angles contain $\beta_{0,-1}$, and red square markers correspond to the case when they do not.

J. Acoust. Soc. Am. **151** (5), May 2022

Abderahmane *et al.* 2873

which implies $D_\beta^m = 0$ for two directions ($100°$ and $10°$). Consequently, α_0 can be easily retrieved ($\alpha_0 = \beta_0 - 45°$).

In practice, due to the discrete nature of the variation of the projection angles (β), it is unlikely that some of these values coincide with the angles $\beta_{0,-1}$. Therefore, D_β cannot be exactly null but is still at its smallest when $\beta \approx \beta_{0,-1}$. A simple algorithm can be designed to find values minimizing D_β^m, allowing a good approximation of α_0 to be found. In essence, the algorithm starts by using the four angles corresponding to the four smallest values of D_β^m to obtain the lower and upper bounds of α_0, and then it tests for different values within these bounds. The red circular markers in Fig. 7 show the case where $\alpha_0 = 52°$ (σ_1 and σ_2 maps remained the same) for which $\beta_{0,-1}$ are not among the tested projection angles. The directions of the minimal values of D_β^m are easily identified, allowing one to obtain α_0. The results for the uniform stress orientation are not given to avoid redundancy as σ_1 and σ_2 can be reconstructed with the same precision as that of σ_1 in the uniaxial case (Fig. 5).

2. Nonuniform stress orientation

Let us now treat the general case where the stress orientation α depends on the position. Without loss of generality, one can write $\alpha(x_1, x_2) = \alpha_0 + c\alpha_1(x_1, x_2)$, where α_0—called, here, the background value—is independent of the position and may be zero, α_1 has a random spatial distribution [in the present example, such a distribution is identical to that in Fig. 5(e)] of magnitude in $[-1°, 1°]$, and c is a constant. To study the consequence of having a nonuniform stress orientation on the reconstruction of σ_1 and σ_2, two simulations were conducted. The different maps of σ_1, σ_2, and α_1 are identical in both simulations and $\alpha_0 = 63°$. In the first simulation, $c = 20$ and in the second simulation, $c = 50$.

The reconstruction of σ_1 and σ_2 starts with the identification of α_0. For this, the approach introduced in the previous paragraph is followed. Once α_0 is found, σ_1 and σ_2 are reconstructed in the same manner as used previously [using Eq. (27)]. In both simulations, the accuracies of the reconstruction of σ_1 and σ_2 are the same so that only the results

for σ_1 are given [Figs. 8(a)–8(c)] for $c = 20$. Figure 8(d) compares along a single ray the original distribution (black solid line) with its reconstruction for $c = 20$ (red solid line) and $c = 50$ (red dotted line). The error [Fig. 8(c)] can reach 25% in R and exhibits geometric patterns stemming from the use of the parallel-beam reconstruction algorithm. The reconstructed map gives the overall spatial distribution. In Fig. 8(d), the effect of deviating from α_0 is clear: for $c = 50$, the difference between the object and its reconstruction can reach 70%. Additional simulations were conducted for lower values $c = 5$ (respectively, $c = 10$) for which the overall error between the object (σ_1 and σ_2) and its reconstruction is less than 6% (respectively, 13%). All of these results demonstrate that the present procedure gives accurate results provided that the stress orientation does not vary greatly. It is worth noting that the map of α could not be reconstructed from σ_1 and σ_2. This is a subject for future work.

Finally, the triaxial case is solved in a manner similar to that for the in-plane biaxial case, the acoustoelastic law is given by Eq. (6). The only difference consists in using an extra measurement (three modes instead of two in the biaxial case or two modes with one being generated at two different centre frequencies). This allows reconstructing σ_3—in principle, with arbitrary precision—using an expression identical to that in Eq. (22). Once σ_3 is known, the problem is brought down to the in-plane biaxial case.

VI. CONCLUSION

A method for stress characterization by means of elastic guided waves has been proposed. The method (M) is nondestructive and takes advantage of the dispersive and multimodal nature of Lamb and SH guided waves to characterize the stress tensor, a multivariable object. Its development was carried out in two steps. In the first step, an An-AEM was derived from previous work by the present authors (Ref. 21). Such model predicts the AEE induced by triaxial stress for a given mode as a function of stress components (σ_1, σ_2, and σ_3), its orientation (α), wave propagation direction (β), and three parameters, the so-called AECs.
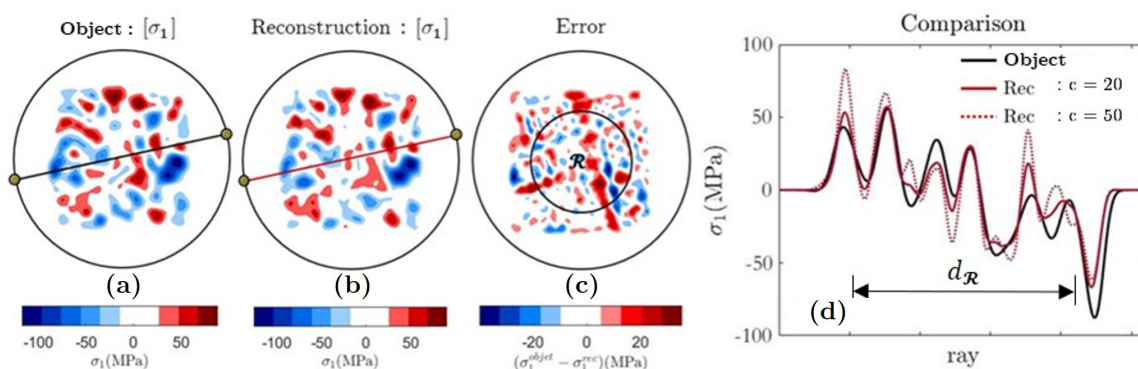
FIG. 8. (Color online) (a) The original σ_1 distribution, (b) its reconstruction using the *parallel-beam* (30 projections and 35 rays), (c) the error between the two for $c = 20$ and (d) their comparison along a single direction [black line in (a) and red line in (b)] of the object and its reconstruction for $c = 20$ (red solid line) and $c = 50$ (red dotted line) are shown.

The AECs are independent of stress and are specific to each mode. Once the domain of validity (frequency range) of the An-AEM has been identified, the inverse problem of characterizing triaxial stress uniform in the plane and through the plate thickness can be solved. Its solution is found using three transducers forming an isosceles right triangle. In the second step, the inverse problem where the stress is nonuniform in the plane but uniform through the thickness is treated. To solve it, the method M uses the TOF SRT. The An-AEM constitutes the physical law to be inverted on each ray to allow for stress reconstruction from TOFs. To define the domain of applicability of M, five cases of increasing complexity were studied. In the first case of uniaxial out-of-plane stress, the scalar unknown σ_3 can be reconstructed with arbitrary precision using the classical tomographic approach. In the second case of uniaxial in-plane stress, the use of two modes on every ray permits the reconstruction of σ_1 with arbitrary precision, whereas the precision for the local stress orientation α depends on how much it varies on a given ray. In the third case of biaxial in- and out-of-plane stress, σ_1 and σ_3 can be reconstructed with arbitrary precision using two modes with one being generated at two different frequencies. The reconstruction of α remains dependent on how much it varies on a given ray. In the fourth case of in-plane biaxial stress and if α is constant, the *parallel-beam* algorithm can be used to reconstruct σ_1 and σ_2 with arbitrary precision. If α varies, only $\sigma_1 + \sigma_2$ can be reconstructed with arbitrary precision, whereas the reconstructions of σ_1 and σ_2 depend on spatial variations of α: the more it varies, the less accurately σ_1 and σ_2 are reconstructed. The last case of triaxial stress is solved in a way similar to that of the in-plane biaxial case, where σ_3 is first reconstructed with arbitrary precision.

The method M represents a necessary step in the solution of the complete problem (p) in which the stress tensor is nonuniform in the plane and through the thickness.

In practice, implementing the method described herein requires the use of transducers that allow efficient mode selection. The modes considered are either Lamb or SH guided waves, and electromagnetic acoustic transducers (EMATs) that can selectively radiate and sense guided waves without mechanical contact[43] constitute a rational choice to implement the tomographic inversion.

[1]L. D. Landau and E. M. Lifshitz, *Theory of Elasticity*, 2nd ed. (Pergamon, New York, 1975), p. 4.

[2]G. S. Schajer, *Practical Residual Stress Measurement Methods* (Wiley, London, 2013).

[3]P. J. Withers, "Residual stress and its role in failure," Rep. Prog. Phys. **70**(12), 2211–2264 (2007).

[4]A. Mordak and Z. Z. Mańko, "Effectiveness of post-tensioned prestressed concrete road bridge realization in the light of research under dynamic loads," Procedia Eng. **156**, 264–271 (2016).

[5]O. Hatamleh, J. Lyons, and R. Forman, "Laser and shot peening effects on fatigue crack growth in friction stir welded 7075-T7351 aluminum alloy joints," Int. J. Fatigue **29**(3), 421–434 (2007).

[6]R. M. Bozorth, *Ferromagnetism* (Wiley-Interscience, Hoboken, 1964).

[7]R. A. Toupin and B. Bernstein, "Sound waves in deformed perfectly elastic materials. Acoustoelastic effect," J. Acoust. Soc. Am. **33**, 216–225 (1961).

[8]J. Kestens, *The Photoelastic Effect and its Applications* (Springer Berlin, Heidelberg, 1975).

[9]S. Dreier and B. Denkena, "Determination of residual stresses in plate material by layer removal with machine-integrated measurement," Procedia CIRP **24**, 103–107 (2014).

[10]N. Tebedge, G. Alpsten, and L. Tall, "Residual-stress measurement by the sectioning method," Exp. Mech. **13**(2), 88–96 (1973).

[11]L. Shi, A. H. Price, and W. N. Hung, "Use of contour method for welding residual stress assessment," Procedia Manuf. **26**, 276–285 (2018).

[12]A. Niku-Lari, J. Lu, and J. F. Flavenot, "Measurement of residual-stress distribution by the incremental hole-drilling method," J. Mech. Work. Technol. **11**(2), 167–188 (1985).

[13]S. Hossain, C. E. Truman, and D. J. Smith, "Finite element validation of the deep hole drilling method for measuring residual stresses," Int. J. Pressure Vessels Piping **93-94**, 29–41 (2012).

[14]V. I. Monine, J. da Cruz Payão Filho, R. S. Gonzaga, E. K. D. Passos, and J. T. de Assis, "X-ray diffraction technique for residual stress measurement in NiCrMo alloy weld metal," Adv. Mater. Sci. Eng. **2018**, 8986423 (2018).

[15]A. Stacey, H. J. MacGillivary, G. A. Webster, P. J. Webster, and K. R. A. Ziebeck, "Measurement of residual stresses by neutron diffraction," J. Strain. Anal. Eng. **20**, 93–100 (1985).

[16]A. Dahia, E. Berthelot, Y. Le Bihan, and L. Daniel, "A model-based method for the characterisation of stress in magnetic materials using eddy current non-destructive evaluation," J. Phys. D: Appl. Phys. **48**, 195002 (2015).

[17]J. Gauthier, T. W. Krause, and D. L. Atherton, "Measurement of residual stress in steel using the magnetic Barkhausen noise technique," NDT E Int. **31**, 23–31 (1998).

[18]R. B. Thompson, S. S. Lee, and J. F. Smith, "Angular dependence of ultrasonic wave propagation in a stressed, orthorhombic continuum: Theory and application to the measurement of stress and texture," J. Acoust. Soc. Am. **80**, 921–931 (1986).

[19]M. Duquennoy, M. Ouaftouh, J. Deboucq, J. E. Lefebvre, F. Jenot, and M. Ourak, "Characterization of micrometric and superficial residual stresses using high frequency surface acoustic waves generated by interdigital transducers," J. Acoust. Soc. Am. **134**, 4360–4371 (2013).

[20]L. Montalto, N. Paone, L. Scalise, and D. Rinaldi, "A photoelastic measurement system for residual stress analysis in scintillating crystals by conoscopic imaging," Rev. Sci. Instrum. **86**, 063102 (2015).

[21]A. Abderahmane, A. Lhémery, and L. Daniel, "Effects of multiaxial prestress on Lamb and shear horizontal guided waves," J. Acoust. Soc. Am. **149**, 1724–1736 (2021).

[22]H. R. Dorfi, H. R. Busby, and M. Janssen, "Acoustoelasticity: Ultrasonic stress field reconstruction," Exp. Mech. **36**, 325–332 (1996).

[23]R. B. King and C. M. Fortunko, "Determination of in-plane residual stress states in plates using horizontally polarized shear waves," J. Appl. Phys. **54**, 3027–3035 (1983).

[24]L. Pintschovius, "Neutron diffraction methods," in *Structural and Residual Stress Analysis by Nondestructive Methods*, edited by V. Hauk (Elsevier Science B. V., Amsterdam, The Netherlands, 1997), Chap. 3, pp. 495–521.

[25]M. K. Khan, M. E. Fitzpatrick, S. V. Hainsworth, A. D. Evans, and L. Edwards, "Application of synchrotron X-ray diffraction and nanoindentation for the determination of residual stress fields around scratches," Acta Materialia **59**, 7508–7520 (2011).

[26]I. Bartoli, A. Marzani, F. Lanza di Scalea, and E. Viola, "Modeling wave propagation in damped waveguides of arbitrary cross-section," J. Sound Vib. **295**(3-5), 685–707 (2006).

[27]M. Hirao, H. Ogi, and H. Fukuokae, "Resonance EMAT system for acoustoelastic stress measurement in sheet metals," Rev. Sci. Instrum. **64**, 3198–3205 (1993).

[28]M. L. Smith and F. Dahlen, "The azimuthal dependence of Love and Rayleigh wave propagation in a slightly anisotropic medium," J. Geophys. Res. **78**, 3321–3333, https://doi.org/10.1029/JB078i017p03321 (1973).

[29]L. Thomsen, "Weak elastic anisotropy," Geophysics **51**, 1954–1966 (1986).

[30]F. Shi, J. E. Michaels, and S. J. Lee, "*In situ* estimation of applied biaxial loads with Lamb waves," J. Acoust. Soc. Am. **133**, 677–687 (2013).

[31]J. R. Asay and A. H. Guenther, "Ultrasonic studies of 1060 and 6061-T6 aluminum," J. Appl. Phys. **38**, 4086–4088 (1967).

J. Acoust. Soc. Am. **151** (5), May 2022

Abderahmane *et al.*   2875

[32]K. Jassby and D. Kishoni, "Experimental technique for measurement of stress-acoustic coefficients of Rayleigh waves," Exp. Mech. **23**, 74–80 (1983).

[33]V. Červený, "Seismic ray theory," in *Geophysics. Encyclopedia of Earth Science* (Springer, Boston, 1989).

[34]A. Javaherian, F. Lucka, and B. T. Cox, "Refraction-corrected ray-based inversion for three-dimensional ultrasound tomography of the breast," Inverse Probl. **36**, 125010 (2020).

[35]A. C. Kak and M. Slaney, *Principles of Computerized Tomographic Imaging* (IEEE, New York, 1988).

[36]S. R. Deans, *The Radon Transform and Some of Its Applications* (Wiley, New York, 1983).

[37]H. Choi and J. S. Popovics, "NDE application of ultrasonic tomography to a full-scale concrete structure," IEEE Trans. Ultrason. Ferroelectr. Freq. Control **62**(6), 1076–1085 (2015).

[38]T. Druet, B. Chapuis, M. Jules, G. Laffont, and E. Moulin, "Passive SHM system for corrosion detection by guided wave tomography," in *Sensors, Algorithms and Applications for Structural Health Monitoring*, edited by B. Chapuis and E. Sjerve (Springer, New York, 2018), pp. 21–29.

[39]D. H. Phillips and J. J. Lannutti, "Measuring physical density with X-ray computed tomography," NDT E Int. **30**, 339–350 (1997).

[40]A. Meléndez, C. E. Jiménez, V. Sallarès, and C. R. Ranero, "Anisotropic *P*-wave travel-time tomography implementing Thomsen's weak approximation in TOMO3D," Solid Earth **10**, 1857–1876 (2019).

[41]A. Mazzullo, E. Stutzmann, J.-P. Montagner, S. Kiselev, S. Maurya, G. Barruol, and K. Sigloch, "Anisotropic tomography around La Réunion island from Rayleigh waves," J. Geophys. Res. Solid Earth. **122**, 9132–9148, https://doi.org/10.1002/2017JB014354 (2017).

[42]H. K. Aben, A. Errapart, L. Ainola, and J. Anton, "Photoelastic tomography for residual stress measurement in glass," Opt. Eng. **44**(9), 093601 (2005).

[43]M. Hirao and H. Ogi, *Electromagnetic Acoustic Transducers—Noncontacting Ultrasonic Measurements Using EMATs* (Springer, New York, 2017), Chap. 3.

2876   J. Acoust. Soc. Am. **151** (5), May 2022

Abderahmane *et al.*